ELSEVIER

Journal of Neuroscience Methods 124 (2003) 83–92

JOURNAL OF NEUROSCIENCE METHODS

www.elsevier.com/locate/jneumeth

Novel functional imaging technique from brain surface with optical coherence tomography enabling visualization of depth resolved functional structure in vivo

R. Uma Maheswari [a], H. Takaoka [b], H. Kadono [c], R. Homma [a], M. Tanifuji [a,*]

[a] *Laboratory for Integrative Neural Systems, Brain Science Institute, RIKEN, 2-1 Hirosawa, Wako, Saitama, Japan*
[b] *Olympus Optical Co. Ltd., Japan*
[c] *Graduate School of Science and Engineering, Saitama University, Saitama City, Japan*

Received 23 August 2002; received in revised form 7 December 2002; accepted 16 December 2002

Abstract

Mapping of the activity of brain by optical intrinsic signal imaging (OISI) provides a two-dimensional activation pattern of visual cortical areas at a resolution of a few hundred microns. However, integration of the intrinsic signal over depth results in loss of finer information about functional organization across the depth. Here, we report the first successful implementation of optical coherence tomography (OCT) at around 30 μm depth resolution to investigate cortical functions of a cat brain in vivo. This technique, named functional OCT (fOCT) provided visually evoked changes in the OCT signal. The fOCT signal shows stimulus specificity that correlates well with that of the intrinsic signals and provides depth resolved layer specific functional information.

Keywords: Optical coherence tomography; Functional optical coherence tomography; Optical intrinsic signal imaging; Primary visual cortex; Scattering change; Visualization of neural activity; Depth resolved functional profile; Volumetric functional imaging

1. Introduction

The activity of the brain is mapped with volumetric techniques such as functional magnetic resonance imaging (fMRI) and positron emission tomography (PET) and they provide a spatial resolution of around a few mm (Toga and Mazziota, 1996). As a complementary technique that can give functional maps at a higher resolution in animal models is optical intrinsic signal imaging (OISI) (Ts'o et al., 1990). This technique measures the reflectance changes from the cortex and it has revealed organizations of functional modules called columns where neurons with similar response properties are clustered together and have dimensions of around a few hundred microns (Bonhoeffer et al., 1991, 1993; Malonek et al., 1994). OISI has also provided some valuable insights in understanding the representations of sensory information in the brain (Wang et al., 1996; Uchida et al., 2000; Tsunoda et al., 2001).

However, OISI has two main disadvantages: (1) as visible wavelengths are used, the penetration depth is limited to a few hundreds of microns and (2) the reflected light is integrated over the depth that results in the loss of information about the organization across depth. Most of the cortex consists of six layers distinguished by cell types and density of cells as shown in Fig. 1. Each layer has specific input and output patterns (Gilbert, 1983). It is also well known that the properties of the cells are different among layers, such as more complex cells exist in layer 2/3 and are orientation selective. Cells in layer 4 are simple and orientation non-selective cells (Hubel and Wiesel, 1962). In OISI, intrinsic signals that originate from secondary metabolic changes due to neural activity, are averaged over these layers.

Here, we report a novel imaging technique for optical imaging of cat brain in vivo with functional optical coherence tomography (fOCT) to visualize depth re-

* Corresponding author. Tel.: +81-48-462-1111; fax: +81-48-462-4696.
E-mail address: tanifuji@postman.riken.go.jp (M. Tanifuji).

0165-0270/03/$ - see front matter
doi:10.1016/S0165-0270(02)00370-9

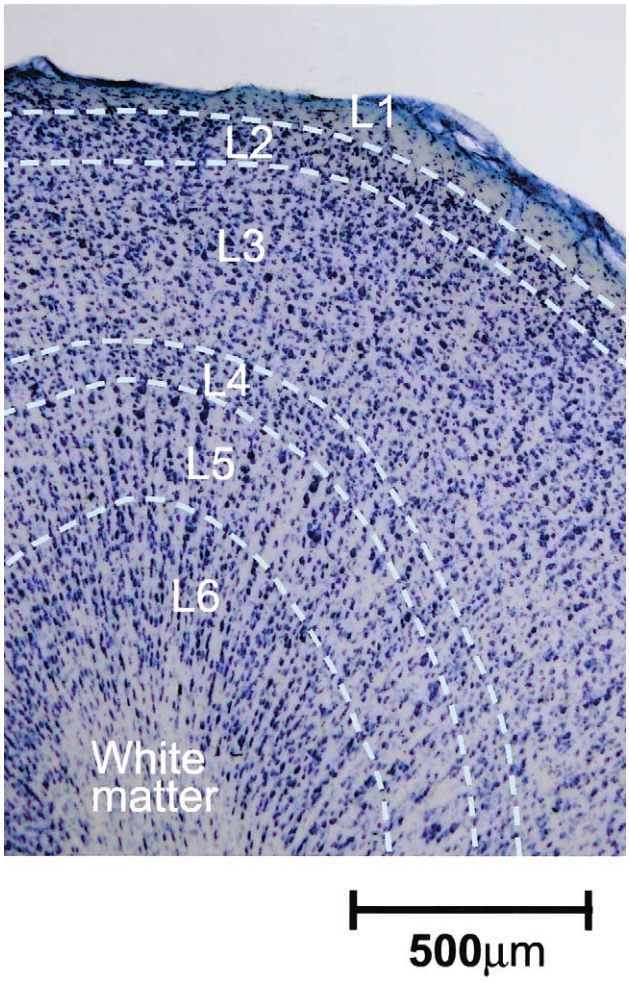

Fig. 1. Nissl stained view of layered structure of cat visual cortex with six layers with layer numbers indicated. Dark dots indicate the cell soma. Layer 1 contains only a few neurons. Layer 2 and layer 3 contain orientation selective neurons while layer 4 contains simple and orientation non-selective cells.

solved functional structure. Further, consistency of fOCT results have been confirmed with the conventional OISI technique. Optical coherence tomography (OCT) is an optical imaging technique where light from a low coherent source is focused onto the tissue and reflectivity of the internal microstructures at different depths is measured by an interferometer (Huang et al., 1991). OCT has been successfully employed for structural imaging of eye (Huang et al., 1991; Siavash et al., 2000; Drexler et al., 2001) non-neuronal tissues such as skin (Yung et al., 1999) and gastrointestinal tissues (Kobayashi et al., 1998). However, its potential in mapping functional signals in the brain remains unexplored. Here we report that OCT can be successfully employed to obtain function related changes of OCT signals from a living animal brain.

2. Methods

2.1. Experimental system

We used fiber based OCT imaging system (Fig. 2). It consists of a Mach–Zehnder type heterodyne interferometer constructed from single-mode fibers for flexibility. Light from a broad-band source (AFC Technologies, Canada) operating at an output power of 30 mW and having a central mean wavelength (λ_o) of 1.31 μm and a spectral width ($\Delta\lambda$) of 50 nm is split into sample and reference beams in the respective ratio of 19:1 by the coupler 1.

Optical frequencies of the sample and reference beams are shifted by acousto-optic modulators (AOM, Asahi glass, Japan). AOMs operate on the principle that when a progressive wave travels inside a crystal, the optical frequencies are shifted due to Doppler effect. By using two AOMs one in the reference path and the other in the sample path, a constant and stable phase delay or frequency difference can be introduced between the interfering beams. Both the reference and sample beams after passing through the circulators illuminate the reference mirror and cortex, respectively. The reflected light was recombined at the coupler 2. The AOMs used in the reference line and sample line were driven at frequencies of 116 and 116.25 MHz, respectively. These RF signals used for driving the AOM were mixed to generate a reference beat signal to be fed to lock-in amplifier. In the lock-in amplifier, it was mixed with the interfering beat signal to give the phase quadranture components. An interference beat signal that has a beat frequency of 250 kHz is detected only when the path lengths of the interferometer arms are matched to within the coherence length of the source ($4\ (\ln 2)\lambda_0^2/\pi\Delta\lambda$) that is calculated to be 34 μm in free space. Heterodyne detection was done with a lock-in amplifier (EG&G, USA) and the amplitude of the demodulated components was fed into a computer via a 16 bit A/D converter. The reference mirror M was mounted on a motorized stage and scanned at a speed of 2 mm s^{-1} with the number of sampling points being 250, i.e. 250 pixels per line. Our system has a dynamic range of 100 dB.

The probe unit viewing the animal side consists of an objective lens of numerical aperture 0.1 and was also fitted with a CCD camera. This allowed simultaneous viewing of the cortical surface with the introduction of visible light from an auxiliary laser source (wavelength $\lambda = 680$ nm). The whole unit was mounted on a manipulator unit that has five degrees of freedom of translation along three axes and rotation and tilt. The flexibility was needed for making the probing light beam normal to the cortical surface and this was adjusted by making the whole field of view to be under focus.

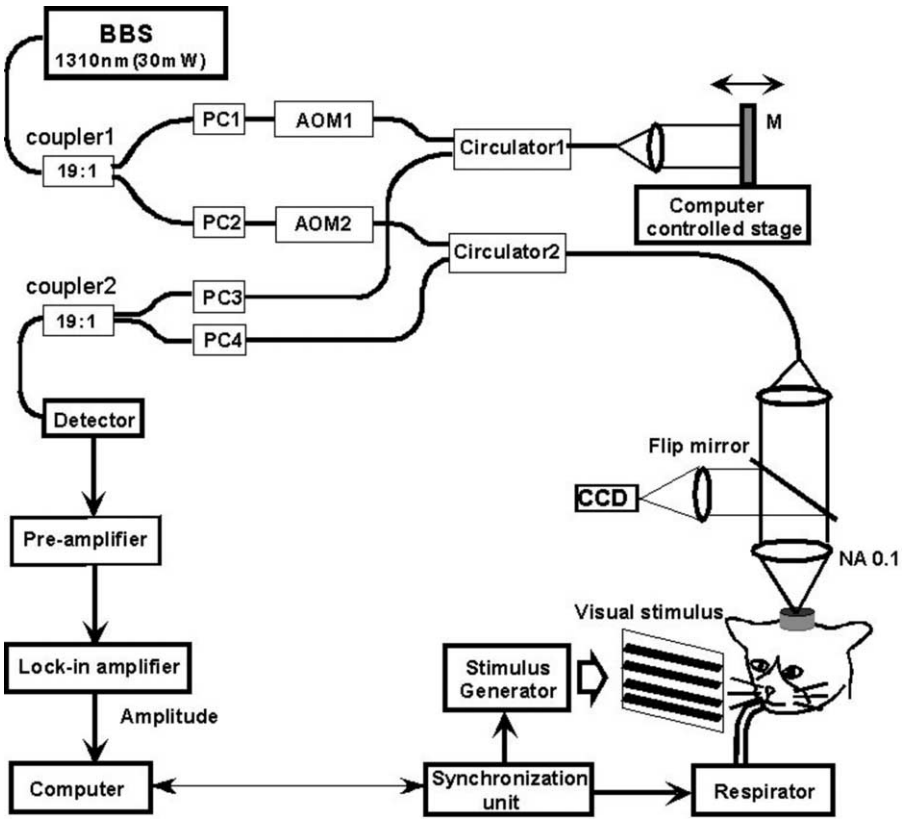

Fig. 2. Experimental system of OCT to obtain differential OCT signal from cat visual cortex. In the figure, the abbreviations denote: BBS, broad band source; AOM, acousto optic modulator; PC, polarization controller, M, mirror and O, objective lens. The probe unit illuminating the cortex is fitted with a CCD camera for simultaneous viewing of the cortical surface. The numerical aperture of the objective lens is 0.1. The polarization controllers (PC1–PC4) were used to maximize the output interference beat signal at the detector.

The main concern when we constructed an interferometer is movement related noise. We tried to minimize our noise fluctuations to less than 1% while the animal related noise was much larger. The animal related fluctuation in the signal had been reduced by conducting measurements in synchronization with heart beat and respiration and keeping the brain surface immobile by using agarose.

2.2. Animal and surgery details

Cat was anesthetized with a mixture of 70% N_2O and 30% O_2 supplemented with 1–2% isoflurane and was paralyzed with pancuronium bromide (0.2 mg kg^{-1} h^{-1}) and was artificially ventilated by a respirator unit. The head of the animal was attached with a metal holder. The holder was attached firmly to a metal rod. A stainless steel chamber (18 mm inner diameter) was fixed onto the skull with dental acrylic cement by aseptic surgery and was placed above area 18 (ca. anterior A10 and posterior P5 in Horsley–Clarke coordinate). Contact lenses were fitted to eyes to protect cornea from drying. The pupils of the eyes were dilated with 0.5% tropicamide and 0.5% phenylephrine hydrochroride so as to induce neural activity over the whole of the retina. After careful removal of the dura matter, inside of the chamber was filled with 1.2% agarose (Agarose-HGS, Nacalai tesque, Japan, Gel strength 1.5%) containing dexamethazone and antibiotics and was sealed with a round glass cover slip and a silicon gasket. After the procedure of chamber fixation and removal of dura matter, the animal was returned to the cage and a gap of around a week was given before OCT experiments for the cortex to recover from the metabolic changes due to exposure. Rectal temperature, ECG and expired CO_2 were continuously monitored during both OCT experiments and surgery.

The experimental protocol was approved by the Experimental Animal Committee of the RIKEN institute that follows the guidelines of the National Institute of Health.

2.3. Stimuli and data acquisition timings

The stimuli were the same as that used for OISI and consisted of square-wave gratings (white = 8 cd m^{-2}, black = 0 cd m^{-2}) having a spatial frequency of 0.15 cycle per degree and moving at a velocity of 15° s^{-1}. The stimulus set consists of five patterns with control or blank (mean luminance 4 cd m^{-2}), horizontal (0°),

vertical (90°) and oblique gratings (45, 135°) and were shown in a sequential order. All stimuli were generated with a VSG2/3 graphics video board (Cambridge Research Systems, UK). The center of the visual field was roughly estimated by projecting images of optic disks onto a screen in front of the animal. The distance of the CRT screen (200–300 mm) was adjusted to have the best focus of optic disks and surrounding vessel patterns.

The stimulus presentation and data acquisition were done at the following timings as shown in schematic of Fig. 3: a total of 40 trials had been done for each stimulus. In a single trial, data acquisition was done for 8 s. After the acquisition onset, stimulus appeared after a delay of 2 s and persisted for 2 s. Within the 8 s interval, the reference mirror was scanned to and fro for a total of 16 times. Inter-stimulus interval was 5 s. The scanning depth fixed as 1 mm was sampled at 4 μm. All data acquisition had been synchronized to the heartbeat and respiration of the cat.

3. Results

3.1. OCT scan results

In order to obtain reflectivity variations from different depths of the cortex, the reference mirror was scanned to change the detection depth in the cortex. The resulting depth resolved reflectivity profiles are shown in Fig. 4. Here, the light beam was adjusted to incident normal to the cortical surface and at a position of interest in relation to the cortical surface. Focusing on to the surface results in an almost exponential decay inside the tissue (red line). On shifting the focus to 300 μm below the surface results in a decay containing additional peaks around the focusing depth. Further we can note that the relative magnitude of the reflectivity close to 1 mm gets stronger. Taking into account the thickness of cortical layers in visual cortex, the measurement covers at least layers 1–3. Although at present, our scan range is confined to superficial layers, we expect

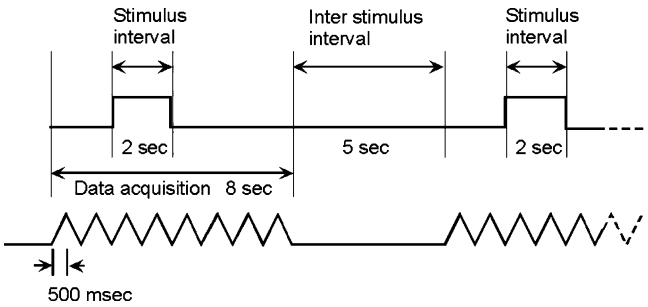

Fig. 3. A schematic diagram to explain the data acquisition protocol with stimulus and scan timings.

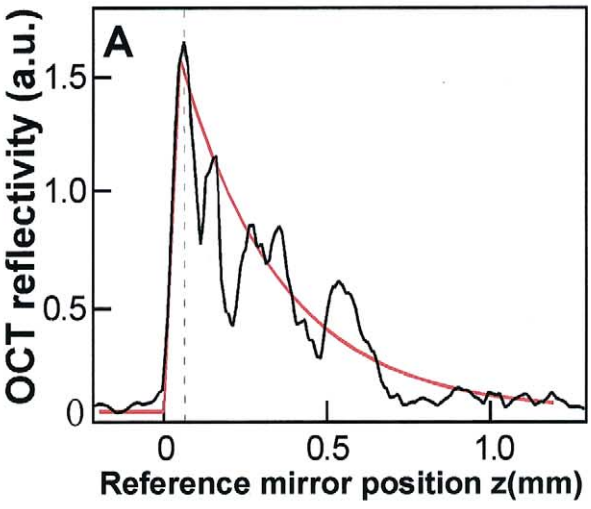

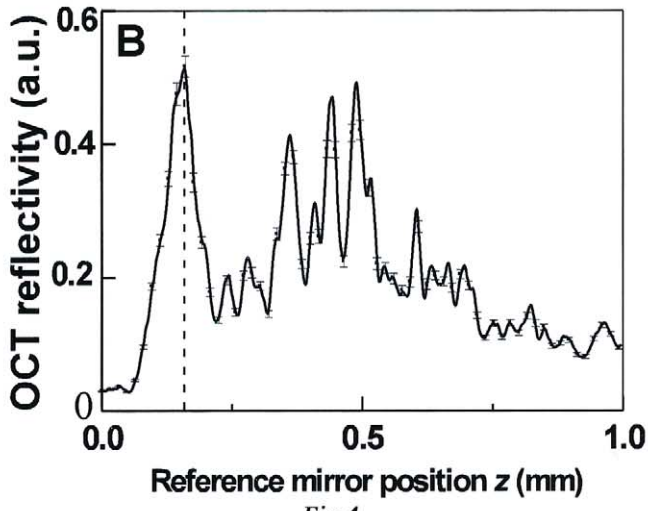

Fig.4

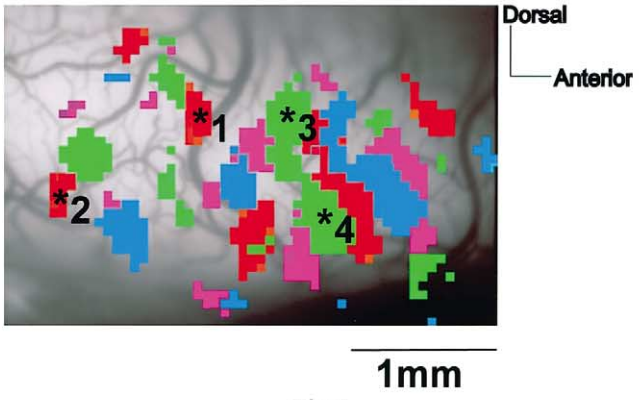

Fig.5

employing high-powered pulsed laser sources could extend the probing depths to a few mm.

The most critical factor that has to be considered in the current study of application of OCT to functional imaging in brain is the question of neural activities eliciting a definitive change in the OCT reflectivity

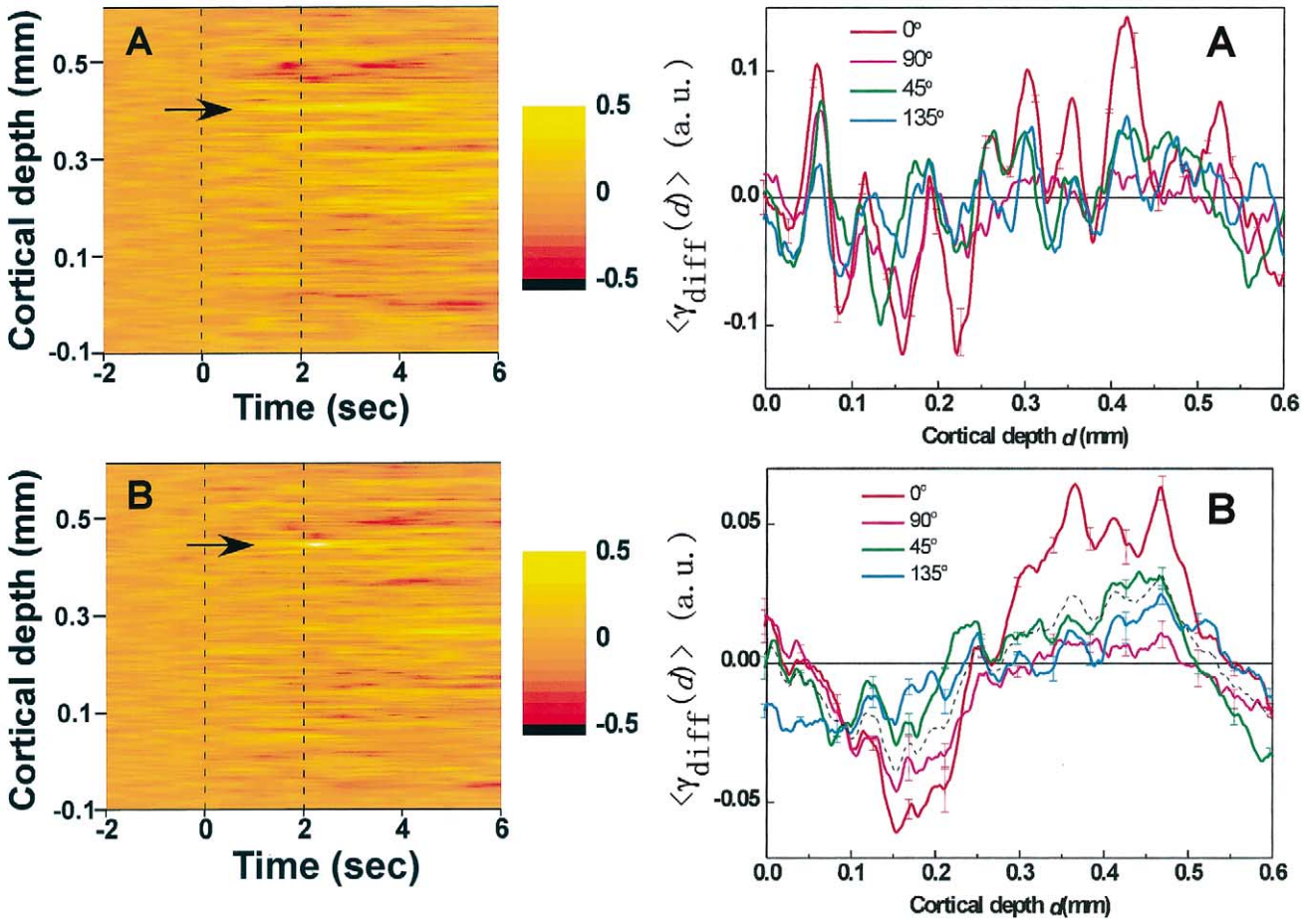

Fig. 6. Spatio-temporal patterns of the differential fOCT signal $\langle \gamma_s\ (d,\ t)\rangle$ in pseudo color coded images obtained from site #1 of Fig. 5 for horizontal grating (A) and vertical grating (B) stimulus. The color scale bar on the right indicates the difference between the ratio $\langle \gamma_s\ (d,\ t)\rangle$ of the grating stimulus and that of the blank or the control. Here abscissa represents time and the ordinate represents the cortical depth. The stimulus duration is indicated by the dotted lines. Arrows indicate the approximate response onset. To avoid motion related noise appearing below 0 of d, cortical surface position was adjusted to fall at around 100 μm.

Fig. 7. Temporally averaged differential OCT signals $\langle \gamma_{\mathrm{diff}}\ (d)\rangle$ for four different grating stimuli as a function of the cortical depth d after passing through a moving average filter of size 40 μm for (A) and 200 μm for (B). The different colored lines red, purple, green and blue lines correspond, respectively, to horizontal (0°), vertical (90°)and oblique orientations (45°, 135°) grating stimuli. Dotted line in (B) indicates the response averaged over all four orientations. Here error bars denote S.E.M. To have clarity, error bars for only horizontal grating stimulus (0°) is shown. Moving averaging filter of size 200 μm was used to test the consistency with OISI result.

signal. During neural activation, secondary physiological structural changes such as capillary dilation (Malonek et al., 1997; Fukuda et al., 2002), change in the density of red blood cells (Tomita et al., 1983) and swelling of glial cells (Holthoff et al., 1998) take place. It is critical whether the changes taking place over a microliter detection volume at a certain depth would produce a finite change in the reflectivity of the OCT signal obtained from that depth. We expected that the secondary physiological changes would produce changes in scattering characteristics that will result in an activity dependent reflectivity change. We call this as functional

Fig. 4. Variation of the OCT reflectivity signal obtained from two different cortices as a function of the reference mirror position (z) when the focus of the objective lens was (A) on the surface and (B) 300 μm below the surface. Red line in A indicates exponential curve ($\exp(-\mu z)$) fitted to the signal where the decay constant μ is 3 mm^{-1}. The dotted line drawn across the sharp peak in B is taken as the cortical surface and fixed as zero. The focus position aligned to deep inside the tissue was used during functional imaging. Note with shifting of the focus to deeper in the tissue, the shape of the decay deviates from exponential type. Error bars of B denote standard error of mean (S.E.M.).

Fig. 5. OISI result showing the image of the cortical surface with statistically significant activated regions of significance level P-value of 2.5×10^{-5} shown in different colors for different grating stimuli. Red, purple, green and blue activation patches correspond, respectively, to horizontal (0°), vertical (90°), oblique gratings 45 and 135°. Four different sites denoted by asterisk and indicated through numbers 1–4 were the sites of OCT depth scan.

OCT signal (fOCT signal) and the technique as fOCT. Prior to the demonstration of fOCT, the functional map was obtained with conventional OISI.

3.2. Intrinsic signal imaging

Extracellular recordings and recent OISI studies showed that neurons responding to the same orientation are clustered and form an orientation map across the cortical surface (Ts'o et al., 1990; Bonhoeffer et al., 1991). The orientation map was obtained with OISI (Fig. 5) under the presentation of different oriented grating stimuli to the animal. During the recording of optical intrinsic signals, the exposed cortex was illuminated with light from an incoherent source having a wavelength of 607 nm. The reflected light was imaged onto a commercial CCD camera by a tandem lens system to be analyzed for stimulus evoked reflectance changes. The different colored patches such as red, purple, green and blue patches correspond to the statistically significant areas activated for horizontal (0°), vertical (90°) and oblique orientations (45, 135°) of the grating stimulus. Four different sites denoted by asterisk and indicated through numbers were the sites of OCT depth scan.

3.3. fOCT signals and data analysis

OCT scan data were obtained at the sites indicated through numbers of Fig. 5. In order to quantify the functional signal obtained, we define the following.

For a single stimulus, we obtained a total of 640 scans. To compensate for the small variations in the surface position over different scans, we used correlation analysis (Swanson et al., 1993). Out of these 640 scans, first, we selected an arbitrary scan i with the reflectivity detected as a function of z being $R_s(z, i)$ for a stimulus s. Next, we calculated the correlation between the ith scan and the rest of the scans j using the following Eq.

$$\Omega(\Delta z;\ i,\ j) = \frac{\int_{-\infty}^{\infty} R_s(z,\ i)R_s(z+\Delta z,\ j)\mathrm{d}z}{\sqrt{\int_{-\infty}^{\infty} R_s(z,\ i)\mathrm{d}z \int_{-\infty}^{\infty} R_s(z+\Delta z,\ j)\mathrm{d}z}} \quad (1)$$

This operation gives the position of the correlation peak that corresponds to the amount of shift necessary for the jth profile to be in alignment with the ith profile. Next, the ratio denoted as,

$$\gamma_s(z,\ i) = \frac{R_s(z,\ i)}{(1/4)\sum_{k=0}^{3} R_s(z,\ k)} \quad (2)$$

was calculated for all the grating stimuli and the control condition. Here, each of the aligned ith scan profile was divided by the averaged aligned pre-stimulus scans. k indicates the pre-stimulus scan profile index and it takes a value of 0, 1, 2, 3 as there are four pre-stimulus scans. The division operation in Eq. (2) removes the unchanging common variation and extracts only changes due to visual stimulation. Next, averaging was done over the 40 data sets to get $\langle\gamma_s\ (z,\ i)\rangle$ for scans performed during each stimulus. Averaging over the scan ratios obtained over duration of 1–3.5 s was calculated to be $\langle\gamma_s\ (z)\rangle$. Finally, the differential OCT signal $\langle\gamma_{\mathrm{diff}}\ (z)\rangle$ was calculated as,

$$\langle\gamma_{\mathrm{diff}}(z)\rangle = \langle\gamma_{\mathrm{grating}}(z)\rangle - \langle\gamma_{\mathrm{control}}(z)\rangle \quad (3)$$

With the above equation by subtracting the differential OCT signal of the control, noise fluctuations such as respiration artifact that were locked to the recording, but not to the grating stimulus are removed. As $\langle\gamma_{\mathrm{diff}}\ (z)\rangle$ is a function of depth, it is possible to detect changes in depth direction with a resolution determined by the coherence length of the source.

3.4. Spatio-temporal variation of fOCT signal

Fig. 6 shows the fOCT signal as a function of time t and cortical depth d, $\langle\gamma_{\mathrm{s}}\ (d,\ t)\rangle$, from site #1 for two orthogonal orientations (0 and 90°). Here the cortical depth was calculated as a ratio of the reference mirror position (z) to the mean refractive index of the brain tissue (Wilson et al., 1990). We used a putative value of 1.4 for the tissue. A systematic investigation of the refractive index of the various layers of brain in vivo needs to be done and we plan to do in near future. In the pre-stimulus period, there are no notable changes in the fOCT signal. Beyond the pre-stimulus period, we could observe that both the vertical and horizontal stimuli elicited changes in fOCT signal. The stimulus evoked responses seemed to be relatively strong (more yellow region) for horizontal than for vertical stimulus orientation though not so apparent. The response was confined

Fig. 8. (A–D) Spatially averaged differential OCT signals $\langle\gamma_{\mathrm{diff}}\ (d)\rangle$ as a function of the cortical depth d with different grating stimuli obtained from four different sites. Numbers 1–4 shown in (A–D), respectively, correspond to the respective scan positions 1–4 denoted by an asterisk in Fig. 5. The different colored lines red, purple, green and blue lines correspond, respectively, to horizontal (0°), vertical (90°) and oblique orientations (45, 135°) grating stimuli. Dotted line indicates the response averaged over all four orientations. Here, error bars denote S.E.M. To have clarity, error bars for only the preferred orientation of the recorded site shown. For all the chosen spots, the objective lens was focused to 100 μm below the surface. (E–H) Fluctuation of $\langle\gamma_{\mathrm{diff}}\ (d)\rangle$ for even and odd scans from respective sites of (A–D). To make the comparison easier, the ordinates are kept to be the same as that used in (A–D).

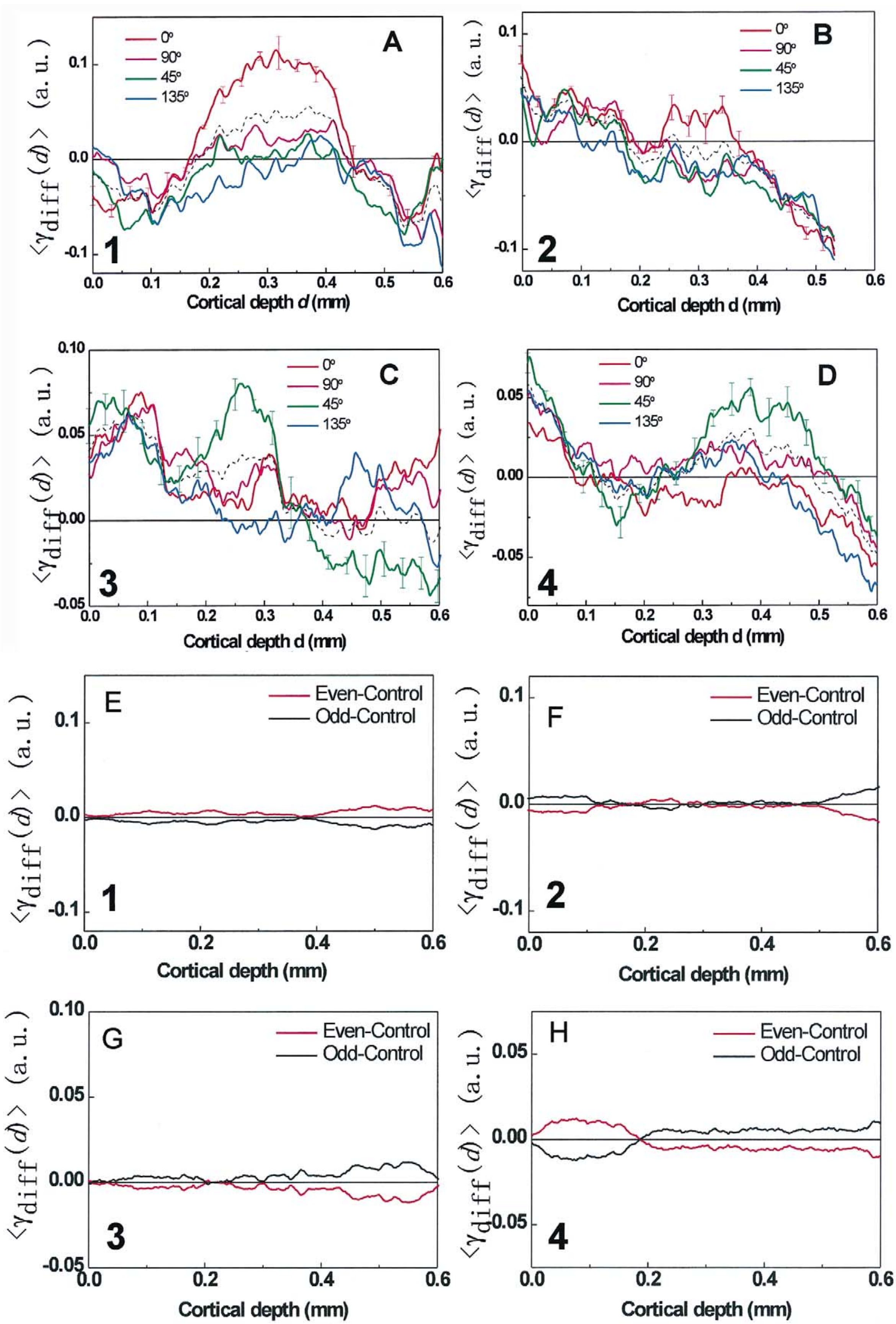
A
B
C
D
E
F
G
H
0°
90°
45°
135°
Even-Control
Odd-Control
⟨γdiff(d)⟩ (a. u.)
Cortical depth d (mm)
Cortical depth (mm)
1
2
3
4

Fig. 8

to a certain range of depth (0.2–0.6 mm). While the response onsets varied across depth, the earliest response onset (arrow) was around 1 s after the stimulus onset and it lasted for a duration of 3–4 s. To visualize the response changes among four different orientations more clearly, we averaged responses obtained over the period of 1–3.5 s from the time stimulus onset that is known to give maximum intrinsic signal change (Malonek et al., 1996).

3.5. Temporally averaged fOCT signal

Temporally averaged differential OCT signal $\langle \gamma_{\text{diff}}(d) \rangle$ obtained as a function of cortical depth d for various grating stimuli is shown in Fig. 7(A). Across the scanned cortical depth of 0–0.6 mm that covers up to most of the layer 2/3, there is a stimulus evoked response in the differential OCT signal $\langle \gamma_{\text{diff}}(d) \rangle$ and it shows depth dependency. The response has a high frequency modulatory component having approximately a period of 0.05 mm. In order to understand the trend of the depth profiles of the signal and also to facilitate comparison with the orientation map given by OISI, we performed moving averaging of $\langle \gamma_{\text{diff}}(d) \rangle$ with a window size of 200 μm (Fig. 7(B)). The resulting depth profile of the response consists of stimulus nonspecific and stimulus specific components.

The envelope of the response profile common to all four oriented stimuli gives the stimulus nonspecific component and is approximated as the response averaged over all four orientations (dotted line in Fig. 7(B)). Here, the stimuli elicited a decrease in the superficial region (0–0.25 mm) and an increase in the middle region (0.25–0.5 mm). We also examined the depth profiles of the responses for four other depth scan positions 1–4 denoted by asterisks of Fig. 5 (Fig. 8(A–D)). In all of these sites, we can observe stimulus nonspecific component as given by the averaged profiles that are not necessarily the same. Right now, the reason for the existence of this stimulus nonspecific component is unclear. A careful consideration is needed to interpret the presence of this stimulus nonspecific component and to associate any physiological significance.

The stimulus specific component is seen specifically in the middle region by horizontal orientation stimulus (Fig. 7(B)). We can see no apparent stimulus specific responses in the superficial region and in the region deeper than the middle region. We can observe similar stimulus specific responses in middle regions for all scan positions (Fig. 8(A–D)). Moreover, the stimulus eliciting this stimulus specific response corresponds to the preferred orientation of that site as determined by OISI (Fig. 5) for all the measured sites. This middle stimulus specific region approximately overlaps with layer 2/3 where the abundant presence of orientation selective cells is known (Hubel and Wiesel, 1962). The superficial regions overlap with layer 1 that lacks visual responsive neurons. Lack of stimulus specific responses in the region deeper than the middle region could be due to both the partial loss of orientation specific cells as the region gets closer to layer 4 and a decrease in signal to noise of the OCT signal itself as this region gets closer to the finishing end of the scan range.

4. Discussion

4.1. Origin of fOCT signal

The origin behind the fOCT signal remains to be investigated. We expect, in fOCT, we could detect neural activity induced local scattering changes happening within a very small volume ($\approx 6000\ \mu m^3$). This scattering change could be the result of changes in the size of the cells or of change in the index variations or of density variations. Here, we assume that the hemoglobin absorption induced changes to be minimal. This is because in the wavelength used the absorption coefficients of oxy and deoxy- hemoglobin are almost the same (Roggan et al., 1999).

It should be pointed out that the OISI and OCT measurements are done at different wavelengths and hence the scattering and the penetration depth are significantly different. But we know that there exists good correlation between the electrical spike activity and the OISI signals measured at around 600 nm. Though our results qualitatively correlate with OISI, we cannot say anything about the spatial extent of our functional signals. Performing surface scans that will give surface maps of the functional organization at near infrared wavelengths along with the depth scans will provide a picture of the overall functional organization. Then we can make some quantitative correlation between the signals obtained under different wavelengths that will hopefully provide some insight into the understanding of neural activity related metabolic changes.

4.2. Reliability of fOCT signal

In order to investigate the fluctuations in the signal, we divided the data obtained for blank into two groups consisting of odd scans and even scans. Next we calculated $\langle \gamma_{\text{diff}}(d) \rangle$ using Eq. (3) where $\langle \gamma_{\text{grating}}(d) \rangle$ could be the sum over either the even or the odd scans. Results of fluctuation $\langle \gamma_{\text{diff}}(d) \rangle$ with respect to the control is shown in Fig. 8 with (E–H) corresponding, respectively, to the different sites (A–D). The fluctuations may be attributed both to that coming from biological as well as the long time fluctuations of the interferometer, which is less than 1%. Our stimulus

specific signals shown in Figs. 7 and 8(A–D) are changes larger than these fluctuations.

4.3. Technological outlook

We demonstrated that OCT technique, which is mainly used for performing structural observation, can be successfully implemented to investigate functional organization of brain. We have confined ourselves to demonstration of a single point. However, by scanning the probe beam with galvano mirrors, it is easier to extend to 3D. We are currently developing such a system that will have the capability for obtaining 3D maps with the micron level resolution both laterally and across depth.

Our OCT system was used to obtain depth resolved layer specific information from visual cortex and is theoretically capable of resolving functional structures up to 17 μm in the depth direction. The depth resolution is mainly limited by the coherence length of the source. Using a source that has a broader spectrum will lead to a higher resolution as well as reduce the effect of speckles. Speckles are a characteristic phenomena that appear when the coherency of light increases and is due to the interference of multiply scattered light from a turbid medium like brain. It is worth to point out that the result of a single OCT scan contains the effect of speckles. These speckles (also called biospeckles) are dynamic due to the random motion of scatterers within the tissue. Temporal averaging greatly reduces the effect of the speckles and, therefore, the averaged results presented in Figs. 4(B), 7 and 8(A–D) are not affected by speckles.

Our proposed novel technique for conducting functional imaging of brain can operate in a complementary way to the widely used and well established single electrode studies and the currently emerging OISI techniques. The former is a single point direct measurement of single neuron activity and can measure discretely across the whole depth and is not capable of mapping the activity from a network of multiple neurons. In contrast, the OISI is an indirect technique capable of mapping the activity simultaneously at micron level resolution from multiple neurons but has the limitation of probing across the depth. Finally, in conclusion, we expect fOCT to be a promising technique capable of delivering results on the working of the brain not only at the cellular but also at the level of network organization.

Acknowledgements

We would like to thank Dr Hongbin Li for his time in preparation of the anatomical sections. Supported in part by Monbukakgakusho grant with grant No. 11750048.

References

Bonhoeffer T, Grinvald A. Iso-orientation domains in cat visual cortex are arranged in pinwheel-like patterns. Nature 1991;353:429–31.

Bonhoeffer T, Grinvald A. Optical imaging of the functional architecture in cat visual cortex: the layout of direction and orientation domains. Adv Exp Med Biol 1993;333:57–69.

Drexler W, Morgner U, Ghanta RK, Kartner FX, Schuman JS, Fujimoto JG. Ultrahigh-resolution ophthalmic optical coherence tomography. Nat Med 2001;7:502–7 (erratum appears in Nat. Med. 2001;7:636).

Fukuda M, Rajagopalan UM, Homma R, Tanifuji M. Contribution of Blood Volume Changes to Intrinsic Optical Signals in International Congress Series. Amsterdam: Elsevier, 2002:897.

Gilbert DC. Microcircuitry of visual cortex. Ann Rev Neurosci 1983;6:217–47.

Holthoff K, Witte OW. Intrinsic optical signals in vitro: a tool to measure alterations in extracellular space with two-dimensional resolution. Brain Res Bull 1998;47:649–55.

Huang D, Swanson EA, Lin CP, Schuman S, Stinson WG, Chang W, Hee MR, Flotte T, Gregory K, Puliafito CA, Fujimoto JG. Optical coherence tomography. Science 1991;254:1178–81.

Hubel DH, Wiesel TN. Receptive fields, binocular interaction and functional architecture in cat's visual cortex. J Physiol 1962;160:106–54.

Kobayashi K, Izatt JA, Kulkarni MD, Willis J, Sivak MV, Jr. High-resolution cross-sectional imaging of the gastrointestinal tract using optical coherence tomography: preliminary results. Gastrointestinal Endosc 1998;47:515–23.

Malonek D, Tootell RB, Grinvald A. Optical imaging reveals the functional architecture of neurons processing shape and motion in owl monkey area MT. Proc R Soc London B Biol Sci 1994;258:109–19.

Malonek D, Grinvald A. Interactions between electrical activity and cortical microcirculation revealed by imaging spectroscopy: implications for functional brain mapping. Science 1996;272:551–4.

Malonek D, Dirnagl U, Lindauer U, Yamada K, Kanno I, Grinvald A. Vascular imprints of neuronal activity: relationships between the dynamics of cortical blood flow, oxygenation, and volume changes following sensory stimulation. Proc Natl Acad Sci USA 1997;94:14826–31.

Roggan A, Friebel M, Dorschel K, Hahn A, Muller G. Optical properties of circulating human blood in the wavelength range 400–2500 nm. J Biomed Opt 1999;4:36–46.

Siavash Y, Rollins AM, Izatt JA. Imaging and velocimetry of the human eye retinal circulation with color Doppler coherence tomography. Opt Lett 2000;51:474–9.

Swanson EA, Izatt JA, Hee MR, Huang C, Lin CP, Schuman JS, Pulfiato CA, Fujimoto JG. In-vivo retinal imaging by optical coherence tomography. Opt Lett 1993;18:1864–6.

Toga AW, Mazziota JC. Brain Mapping: The Methods. San Diego: Academic, 1996.

Tomita M, Gotoh F, Yamamoto M, Tanahashi N, Kobari M. Effects of hemolysis, hematocrit, RBC swelling, and flow rate on light scattering by blood in a 0.26 cm ID transparent tube. Biorheology 1983;20:485–94.

Ts'o DY, Frostig RD, Lieke EE, Grinvald A. Functional organization of primate visual cortex revealed by high resolution optical imaging. Science 1990;249:417–20.

Tsunoda K, Yamane Y, Nishizaki M, Tanifuji M. Complex objects are represented in macaque inferotemporal cortex by the combination of feature columns. Nat Neurosci 2001;4:832–8.

Uchida N, Takahashi YK, Tanifuji M, Mori K. Odor maps in the mammalian olfactory bulb: domain organization and odorant structural features. Nat Neurosci 2000;3:1035–43.

Wang G, Tanaka K, Tanifuji M. Optical imaging of functional organization in the monkey inferotemporal cortex. Science 1996;272:1665–8.

Wilson BC, Jacques SL. Optical reflectance and transmittance of tissues: principles and applications. IEEE J Quantum Elect 1990;26:2186–99.

Yung KM, Lee SL, Schmitt JM. Phase-domain processing of optical coherence tomography images. J Biomed Opt 1999;4:125–36.